Light-Triggered Transformation of Stilbene Supramolecular Polymers: Thermodynamic versus Kinetic Control

Yi Lu,[a] Ruilong Zhang,[a] Zhilong Hong,[a] Pingping Liang,[b]* Rui Liao,[a]*

and Feng Wang[a]*

[a] *Department of Polymer Science and Engineering, University of Science and Technology of China, Hefei, Anhui 230026 (P. R. China). E-mail: drfwang@ustc.edu.cn (F.W.); rliao@ustc.edu.cn (R.L.).*

[b] *School of Life Sciences, Anhui Medical University, Hefei 230032, (P. R. China). E-mail: iamppliang@163.com (P.L.).*

Table of Content

1. *Materials and Methods*

Reagents and reactants: Concentrated hydrochloric acid, 4-dimethylaminopyridine (DMAP), 1-ethyl-3-(3-dimethyl aminopropyl)carbodiimide hydrochloride (EDC·HCl), cuprous iodide (CuI), bis(triphenylphosphine)palladium(II) chloride [Pd(PPh$_3$)$_2$Cl$_2$], *trans*-1,2-bis(4-iodophenyl)ethene were reagent grade and used as received. Compounds **3** [(*S*)-**3** or (*R*)-**3**] were synthesized according to the reported procedures.[S1-S3] Other reagents and solvents were employed as purchased.

Instruments: ^{1}H NMR spectra were collected on a Bruker AscendTM 400 MHz spectrometer with TMS as the internal standard. ^{13}C NMR spectra were recorded on a Bruker AscendTM 400 MHz spectrometer at 101 MHz. MALDI-TOF measurements were recorded on a Bruker Autoflex Speed spectrometer with DCTB as the matrix. UV–Vis spectra were recorded on a Jasco V-730 spectrophotometer. Circular dichroism (CD) measurements were performed on a Jasco J-1500 circular dichroism spectrometer, equipped with a PFD-425S/15 Peltier-type temperature controller. CPL measurements were performed on a Jasco CPL-300 circularly polarized luminescence spectrophotometer. Steady-state emission spectra were recorded on a FluoroMax-4 spectrofluorometer (Horiba Scientific), and analyzed with the Origin (v8.1) integrated software FluoroEssence (v2.2). FT-IR spectra were collected by employing a Nicolet 6700 FT-IR spectrometer. AFM measurements (tapping mode) were performed using a Bruker Dimension Icon with ScanAsyst system in air with silica cantilevers (RFESPA-75, Ohm-cm Antimony (n) doped Si) and a resonance frequency of ~ 75 kHz and a spring constant of ~ 3 N m^{-1}. The images were analyzed using the Pico Image processing program.

Irradiation Methods: Irradiation-based experiments were performed using an LED LED Engin 20 W by ZLUVLAMP at 365 nm. The irradiation experiments ensure that the distance between the light source and the solution is certain (10 cm) so that the irradiation amount per unit time is equal.

DFT calculations: Optimization of the structures was performed using the semi-empirical dispersion-corrected PM6 method as implemented in the MOPAC package.[S4]

Dispersion interactions were considered and all calculations were carried out in a vacuum. The reliability of the optimized structures was checked via frequency calculations based on density functional theory (DFT). There are no imagery frequencies for the optimized geometries. The long side chains were substituted by H atoms to make the calculation feasible. The DFT functional ωB97XD was used, with the adoption of the 6-31G(d) basis set. The molecular orbitals were visualized using the Gauss View 6.0 software.

One-component model for supramolecular polymerization. The thermodynamic parameters of the supramolecular polymerization of (*S*)-**1**, and (*S*)-**2** are acquired by fitting spectroscopy data of melting curves with the one-component model for supramolecular polymerization.[S5] The fitted parameters for the (*S*)-**1** supramolecular homopolymers are the enthalpy of elongation $\Delta H_{(S)\text{-}1}$, the enthalpy of nucleation $\Delta H^n_{(S)\text{-}1}$ and the entropy term $\Delta S_{(S)\text{-}1}$. The entropy term is the same for nucleation and elongation. These parameters are related to the equilibrium constants of the elongation phase by:

$$K_{(S)\text{-}1} = exp\ (-\Delta G_{(S)\text{-}1} / RT) \qquad\qquad \text{Eq. S1}$$

$$\text{with } \Delta G_{(S)\text{-}1} = \Delta H_{(S)\text{-}1} - T\Delta S_{(S)\text{-}1} \qquad\qquad \text{Eq. S2}$$

and of the nucleation phase (with nucleation penalty $NP_{(R)\text{-}1}$) by

$$K^n_{(S)\text{-}1} = \sigma_{(S)\text{-}1} \times K_{(S)\text{-}1} \qquad\qquad \text{Eq. S3}$$

$$\text{with } \sigma_{(S)\text{-}1} = exp\ (NP_{(S)\text{-}1} / RT) \qquad\qquad \text{Eq. S4}$$

$$NP_{(S)\text{-}1} = \Delta H_{(S)\text{-}1} - \Delta H^n_{(S)\text{-}1} \qquad\qquad \text{Eq. S5}$$

The model was fitted to the experimentally obtained melting curves of samples with varying monomer concentrations. The melting curves were divided by the total monomer concentration to weigh all samples equally in the fitting procedure. The fitting parameters used were the entropy and enthalpy of elongation and the nucleation penalty. The entropy was sampled between –0.050 and –0.800 kJ·mol^{-1}·K^{-1}, the Gibbs free energy between –20 and –220 kJ·mol^{-1} to determine the enthalpy and the nucleation penalty between –5 and –35 kJ·mol^{-1}. The lhsdesign function in Matlab was used to create 500 initial parameter sets using Latin hypercube sampling. Each of these initial
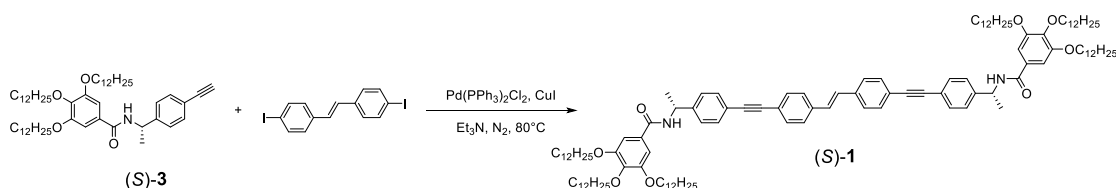
parameter sets was optimized to minimize the sum of squares of the cost vector with the Levenberg-Marquardt algorithm. The Matlab function lanolin was used to minimize the cost vector, selecting the lowest norm of the residual sum of squares.

2. Synthesis routes of the designed compounds
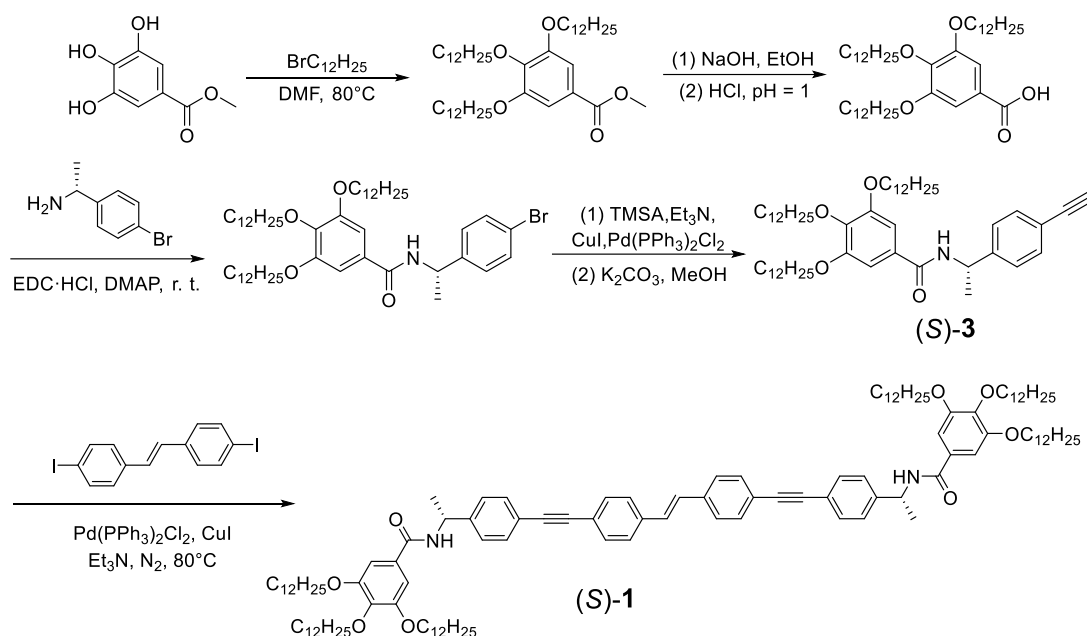

Scheme S1. Synthetic routes toward compounds (*S*)-**1**.

*Synthesis of compounds (S)-**1***

A mixture of *trans*-1,2-bis(4-iodophenyl)ethene (266 mg, 0.50 mmol), (*S*)-**3** (841 mg, 1.1 mmol), $Pd(PPh_3)_2Cl_2$ (18 mg, 0.025 mmol) and CuI (6 mg, 0.03 mmol) were dissolved in Et_3N (10 mL) and THF (20 mL). The reaction mixture was degassed and stirred at 40°C for 20 hours. After cooling down to room temperature, the solvent was evaporated under reduced pressure, and the residue was extracted with $CHCl_3/H_2O$. The combined organic solution was dried over anhydrous Na_2SO_4 and evaporated with a rotary evaporator. The residue was purified by flash column chromatography (petroleum ether/ $CHCl_3$, 2:1; *v/v* as the eluent) to afford compound (*S*)-**1** as a light white solid (445 mg, 50%). ^1H NMR (400 MHz, $CDCl_3$, Fig. S27): δ (ppm) 7.52 (m, 12H), 7.38 (d, *J* = 8.2 Hz, 4H), 7.12 (s, 2H), 6.97 (s, 4H), 6.20 (d, *J* = 7.7 Hz, 2H),5.31 (m, 2H), 3.99 (m, 12H), 1.76 (m, 12H), 1.62 (s, 6H), 1.45 (t, 12H), 1.28 (d, *J* = 7.3 Hz, 96H), 0.87 (t, 18H). ^{13}C NMR (101 MHz, $CDCl_3$, Fig. S28): δ (ppm) 166.6, 153.1, 143.5, 141.5, 137.1, 132.0, 129.3,128.9, 126.6, 126.5, 122.6, 122.4, 105.9, 90.3, 89.7,

76.2, 73.6, 69.5, 58.5, 49.1, 32.2, 30.4, 29.8, 29.8, 29.7, 29.6, 26.2, 22.8, 21.6, 18.5, 13.2. MALDI-TOF: m/z 1804.2 ([M + Na]$^+$, Fig. S29). Calculated MS: m/z 1780.8

*Synthesis of compound (R)-**1***
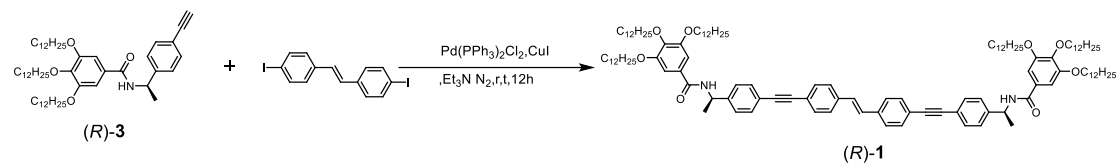
The same procedure was applied to the synthesis of enantiomer compound (R)-**1**, by employing (R)-**3** instead of (S)-**3** as the reactant. (R)-**1** was obtained as a light white solid (110 mg, 25%). ^{1}H NMR (400 MHz, CDCl$_3$): δ (ppm) 7.52 (m, 12H), 7.38 (d, $J =$ 8.2 Hz, 4H), 7.12 (s, 2H), 6.97 (s, 4H), 6.20 (d, $J =$ 7.7 Hz, 2H),5.31 (m, 2H), 3.99 (m, 12H), 1.76 (m, 12H), 1.62 (s, 6H), 1.45 (t, 12H), 1.28 (d, $J =$ 7.3 Hz, 96H), 0.87 (t, 18H). MALDI-TOF: m/z 1804.6 ([M + Na]$^+$, Fig. S30). Calculated MS: m/z 1780.8

3. Supramolecular polymerization of (S)-1
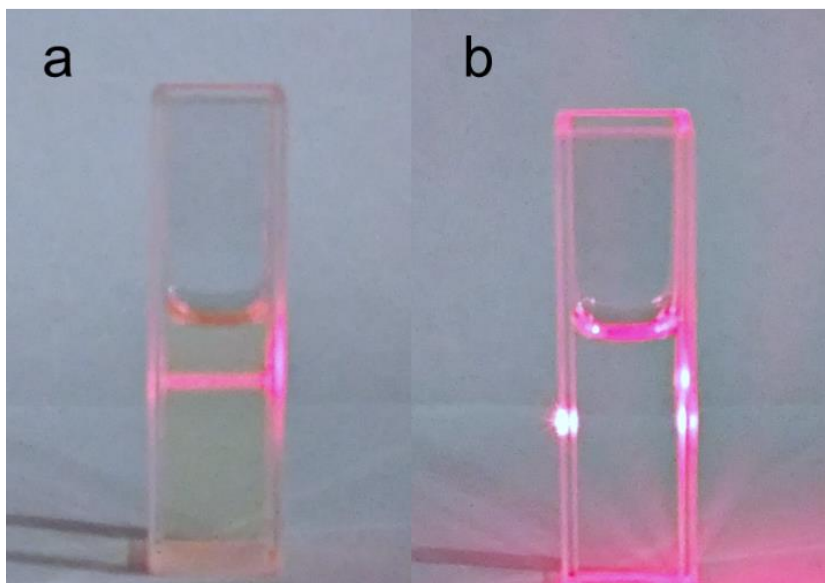
Fig. S1 Tyndall effect images of (S)-**1** in MCH (a) and CHCl$_3$ (b) at 298 K (c = 20 μM). The phenomena suggest the formation of supramolecular assembly of (S)-**1** in MCH.
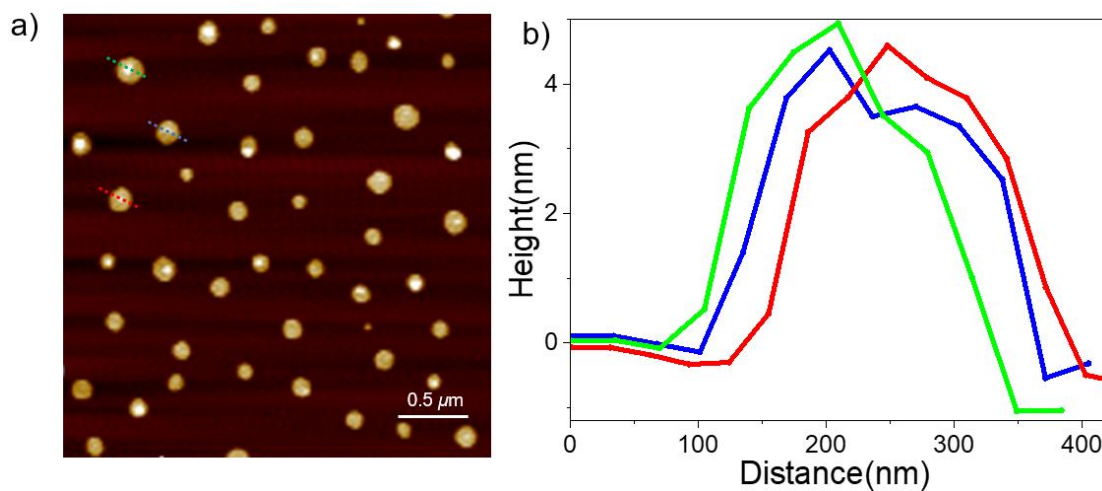
Fig. S2 AFM images of (S)-**1** [prepared by spin coating the sample in MCH (c = 20 μM) into mica]. The average diameter of the individual spheres is around 200-300 nm. Scale bar: 0.5 μm.
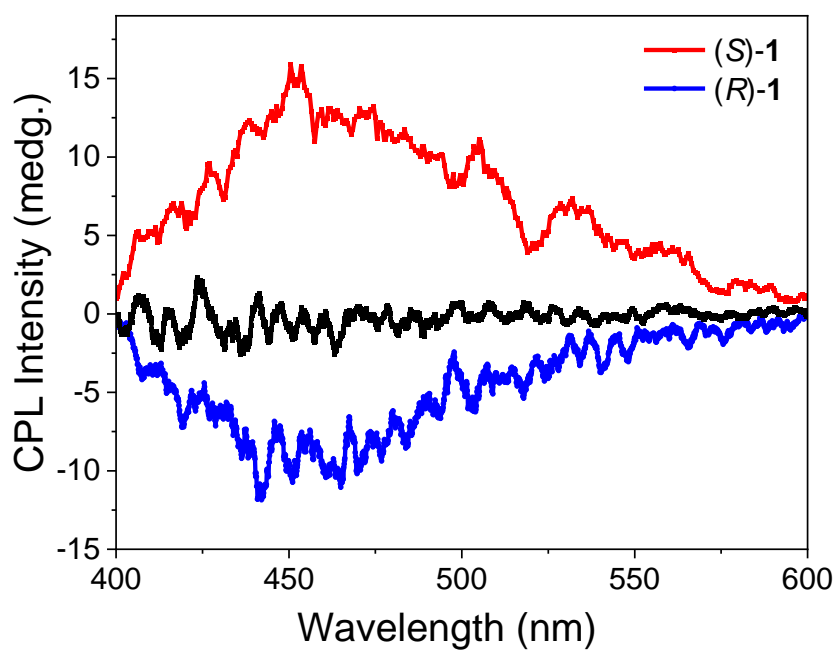
Fig. S3 CPL spectra of (*S*)-**1** and (*R*)-**1** in MCH, together with (*S*)-**1** in CHCl$_3$ (black line, *c* = 20 μM) under 365 nm excitation.
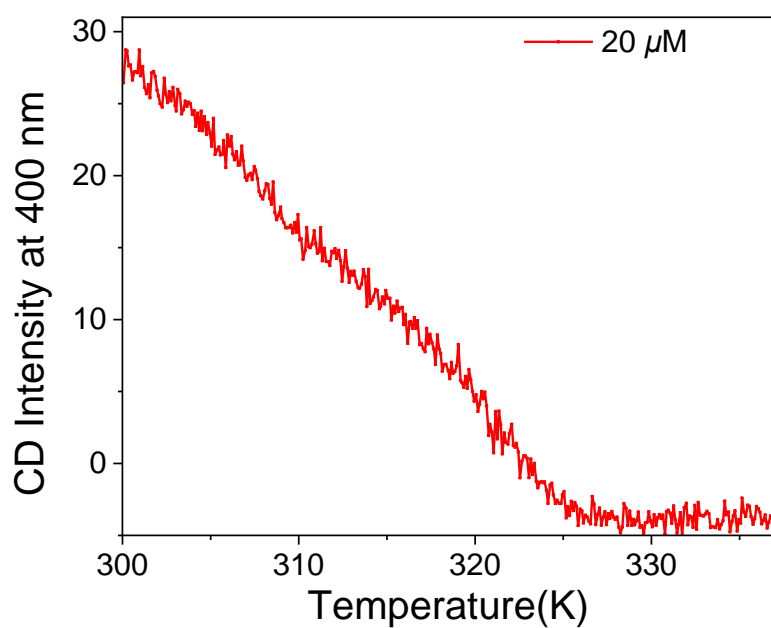
Fig. S4 CD cooling curve of the supramolecular polymerization of (*S*)-**1** in MCH (*c* = 20 μM, CD intensities were shown as absolute values). The cooling rate was 1 K·min^{-1}. The T_e value was determined to be 324.1 K, which is compared to that of the UV-Vis cooling curve.

.
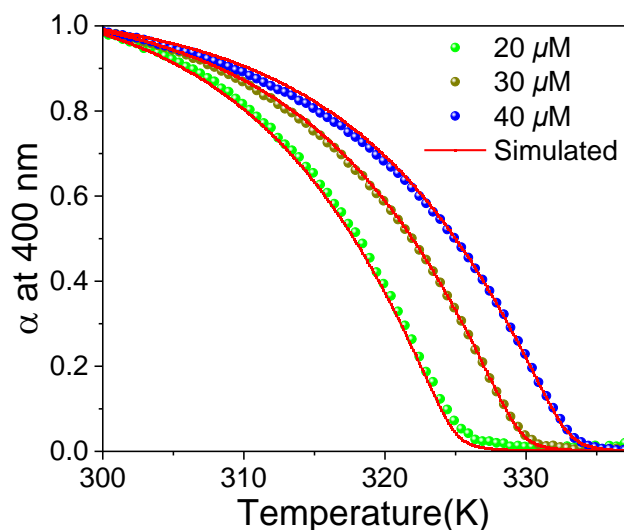
Fig. S5 Experimental (circles) and simulated (lines) cooling curves of the (*S*)-**1** supramolecular polymers at three different concentrations (*c* = 20 *µ*M, 30 *µ*M, 40 *µ*M) in MCH. The cooling rate was 1 K min^{-1}. The $\Delta H_{(S)\text{-}\mathbf{1}}$, $\Delta S_{(S)\text{-}\mathbf{1}}$, $\Delta G_{(S)\text{-}\mathbf{1}}$, were determined to be – 78.1 kJ mol^{-1}, –151 J mol^{-1} K^{-1}, –33.2 kJ mol^{-1} respectively. The thermodynamic parameters are calculated according to Eq. S1–S5.
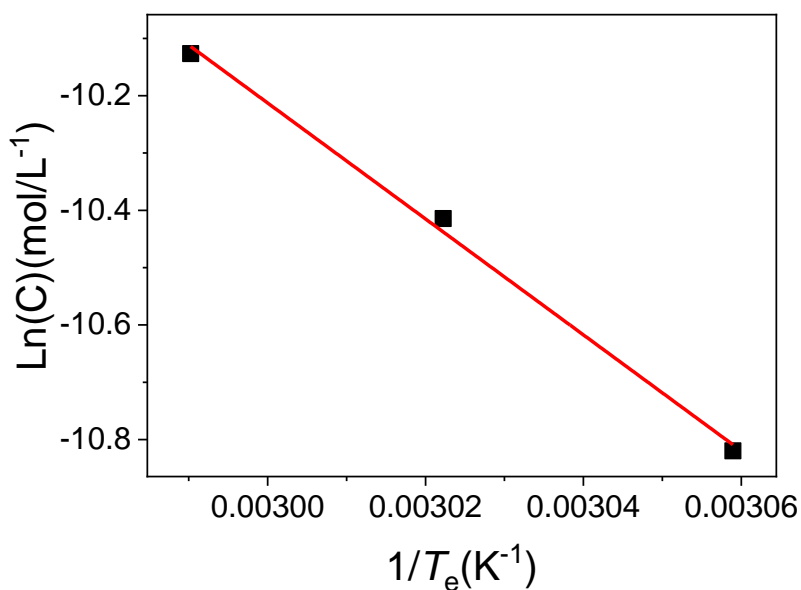
Fig. S6 Van't Hoff plot analysis for the (*S*)-**1** supramolecular polymerization process. The values of $\Delta H_{(S)\text{-}\mathbf{1}}$ and $\Delta S_{(S)\text{-}\mathbf{1}}$ were determined to be –84.1 kJ mol^{-1} and –167.4 J mol^{-1} K^{-1}, respectively.
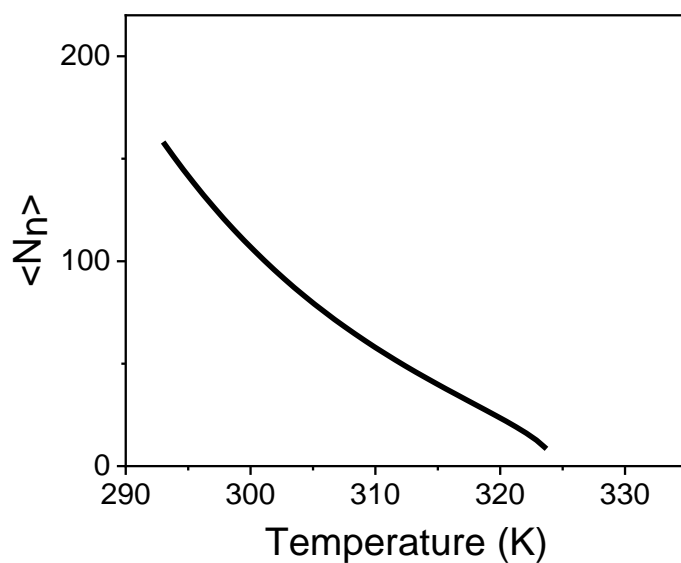
Fig. S7 Simulated number averaged degree of polymerization ($<N_n>$) of (*S*)-**1** ($c = 20\ \mu$M) at various temperatures. The calculation equation of $<N_n>$ follows the previous literature reported by Meijer and coworkers[S6]. The calculated theoretical number-averaged degree of polymerization was 115 at 298 K, verifying the formation of long-range-ordered supramolecular polymers.
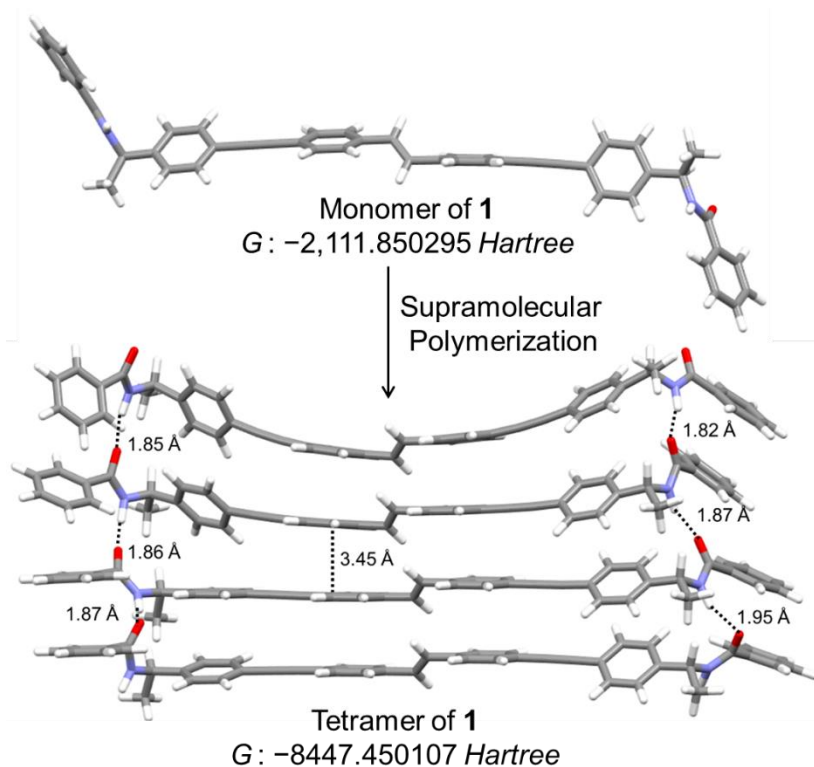
Fig. S8 Optimized structures of **1** and **1₄** based on DFT calculations. The calculated energy of the monomer and tetramer were determined as −2111.850295 Hartree and −8447.450107 Hartree, respectively.
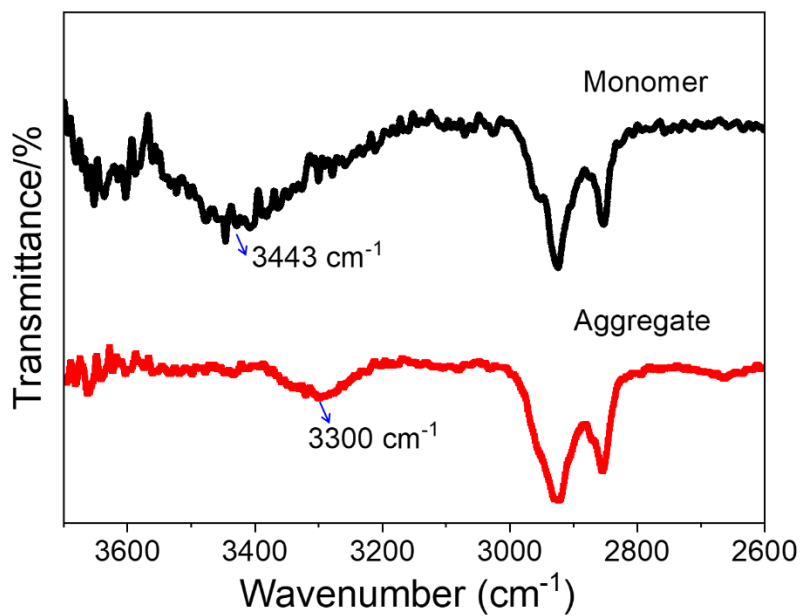
Fig. S9 FT–IR spectra of the N–H stretching vibration of (*S*)-**1** in CHCl$_3$ (black line, monomeric state) and MCH (red line, supramolecular polymeric state) at 298 K (c = 5.00 mM). The N–H stretching bands shift from 3443 cm^{-1} in CHCl$_3$ (the monomeric state) to 3300 cm^{-1} in MCH (the supramolecular polymeric state).

4. *Photo-responsive behavior of (S)-1$_{sp}$*
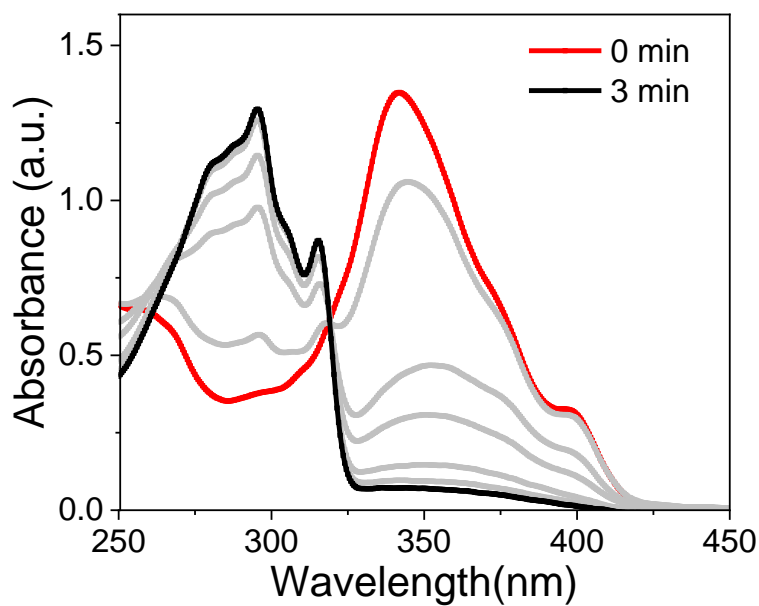
Fig. S10 UV–Vis spectra of (S)-1$_{sp}$ upon the irradiation (365 nm) for 3 min at 298 K ($c = 20$ μM, MCH).
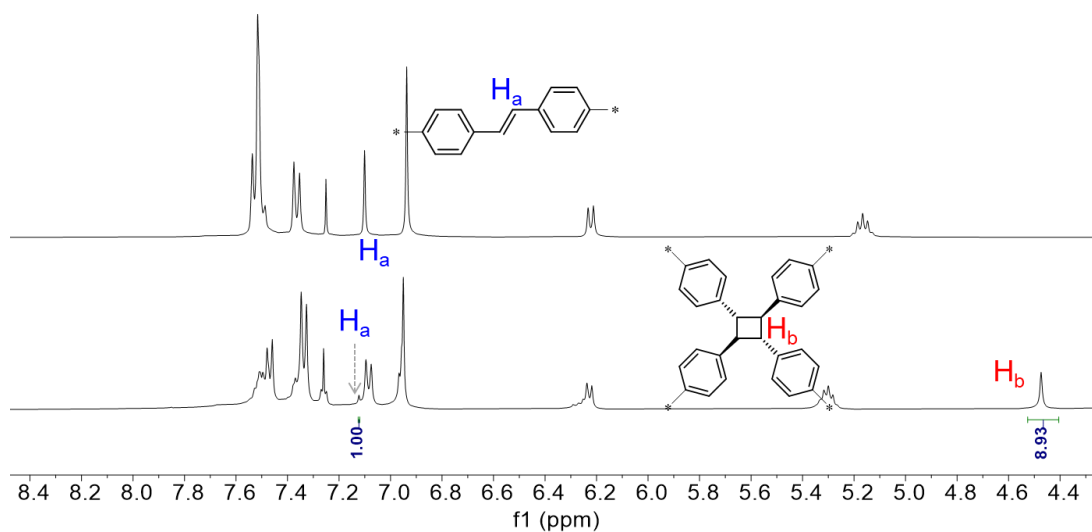
Fig. S11 Partial ^{1}H NMR spectra of (S)-**1** upon light irradiation in MCH for 3 min at 298 K. After irradiation, the MCH solvents were removed, followed by the addition of CDCl$_3$. Analysis of the integration ratio between the ^{1}H NMR resonant signals at $\delta = 7.12$ (vinyl protons) and 4.47 ppm (cyclobutene protons) to obtain the conversion rate of the photo-irradiated.
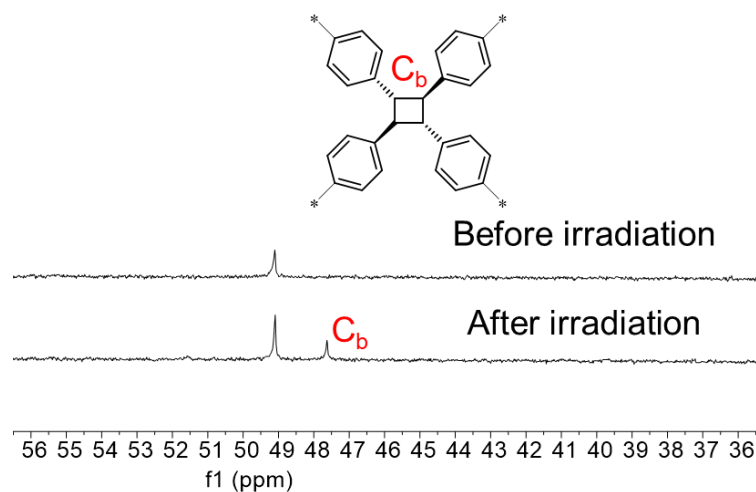
Fig. S12 Partial ^{13}C NMR spectra (400 MHz, CDCl$_3$, 293 K) of (*S*)-**1** upon light irradiation in MCH for 3 min at 298 K. After irradiation, the MCH solvents were removed, followed by the addition of CDCl$_3$. A new signal appeared at 47.6 ppm, which arises from the aliphatic cyclobutene ring.
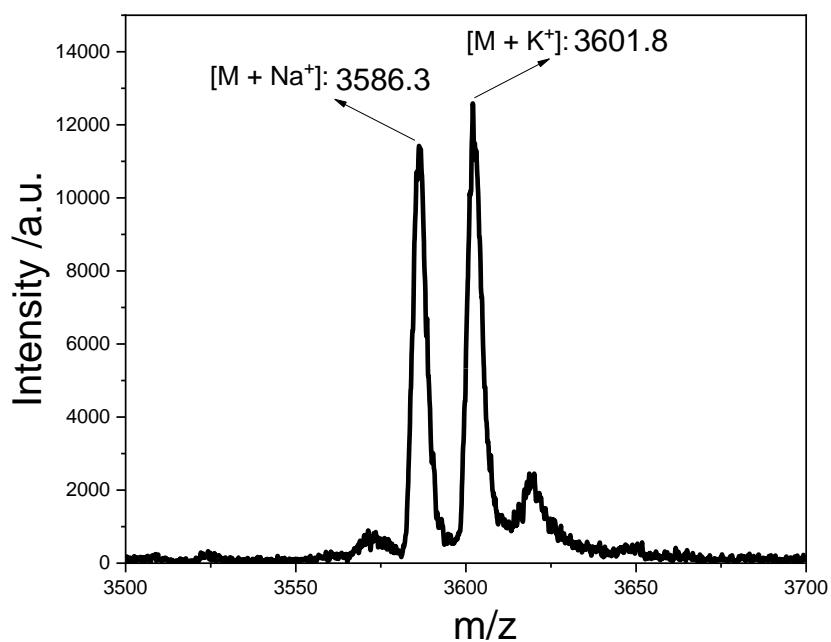
Fig. S13 MALDI-TOF mass spectrum of (*S*)-**2**, which revealed the *m/z* values of 3601.8 ([M + K$^+$]) and 3586.3 ([M + Na$^+$]). It is consistent with a [2 + 2] cycloaddition product of (*S*)-**1**.
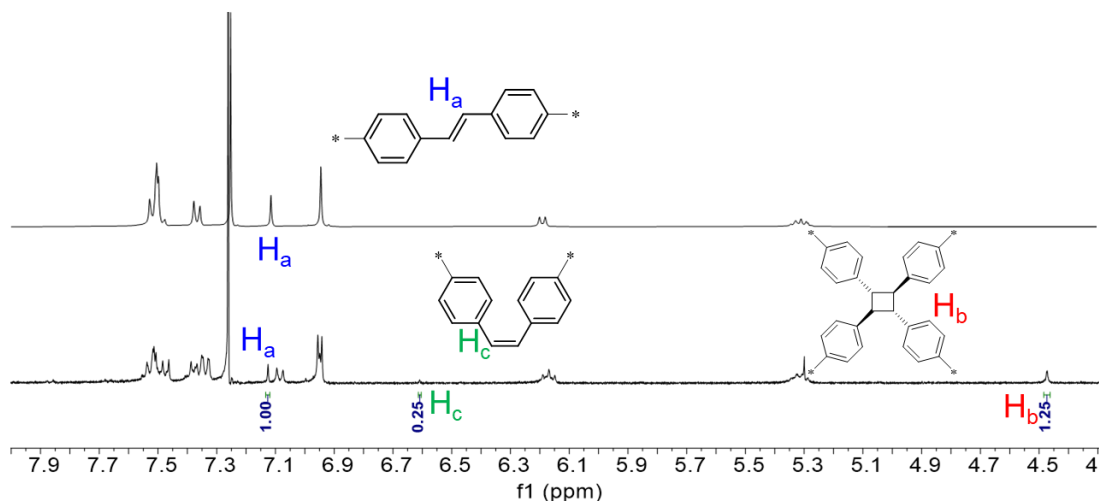
Fig. S14 Partial ^{1}H NMR spectra (400 MHz, CDCl$_3$, 293 K) of (*S*)-**1** upon light irradiation in CDCl$_3$ for 20 min at 298 K. Analysis of the integration ratio between the ^{1}H NMR resonant signals at δ_{trans} = 7.12 (vinyl protons), δ_{cis} = 6.60 (vinyl protons) and 4.47 ppm (cyclobutene protons) to obtain the conversion rate of the photo-irradiated.
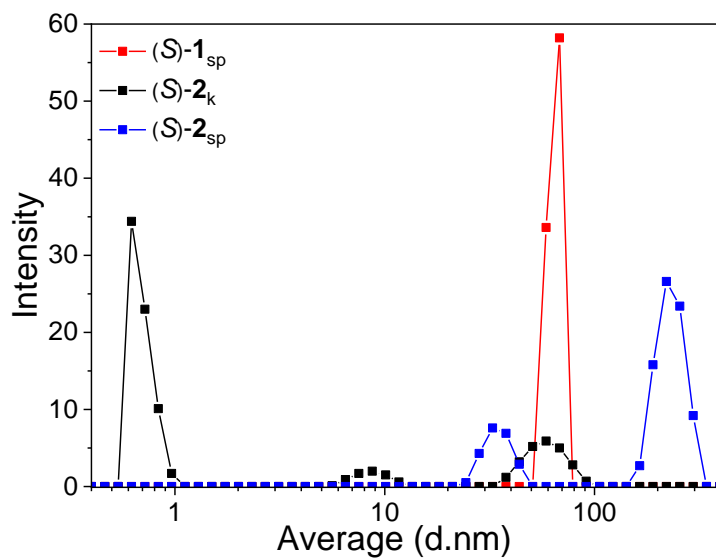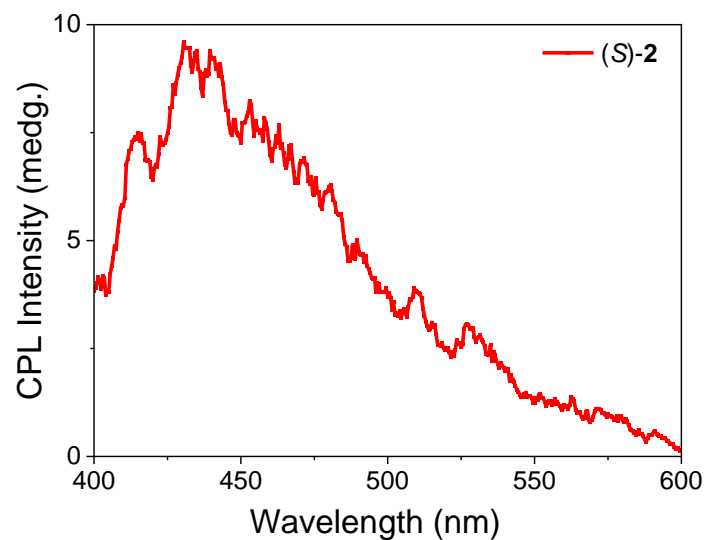

Fig. S15 Dynamic light scattering (DLS) measurements of (*S*)-**1**$_{sp}$ before (red line) and after (black line) light irradiation for 3 min [(*S*)-**2**$_k$], followed by thermal annealing [(*S*)-**2**$_{sp}$].
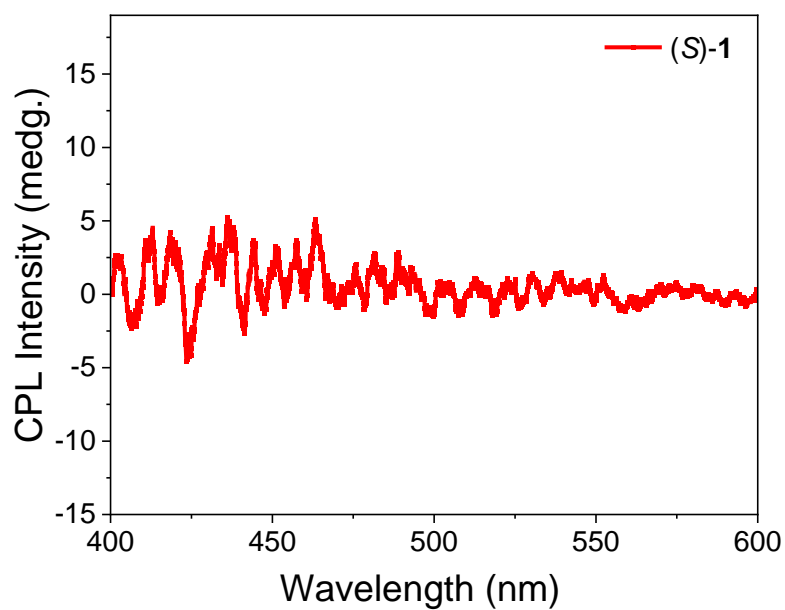
Fig. S16 CPL spectra of (*S*)-**2**$_k$ in MCH (c = 20 μM).
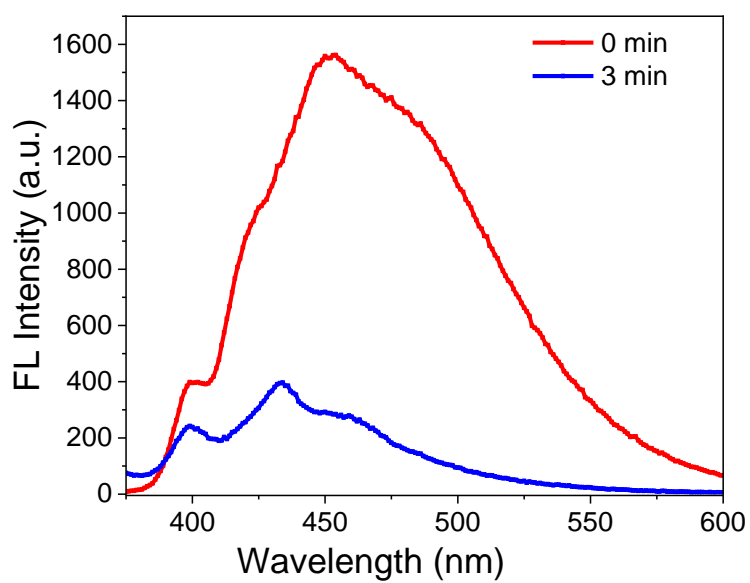
Fig. S17 Fluorescence spectra of (*S*)-**1** upon the light irradiation for 3 min in MCH (*c* = 20 μM) at 298 K.
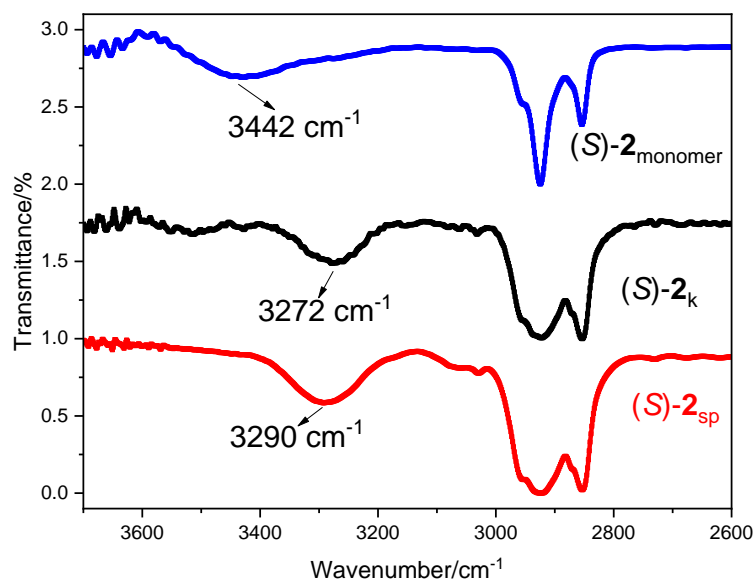
Fig. S18 CPL spectra of (*S*)-**2**sp in MCH (*c* = 20 *μ*M) under 365 nm excitation. The emergence of a blue-colored CPL signal of (*S*)-**2**sp after thermal annealing (by raising the temperature to 353 K and subsequently cooling the solution to 298 K).
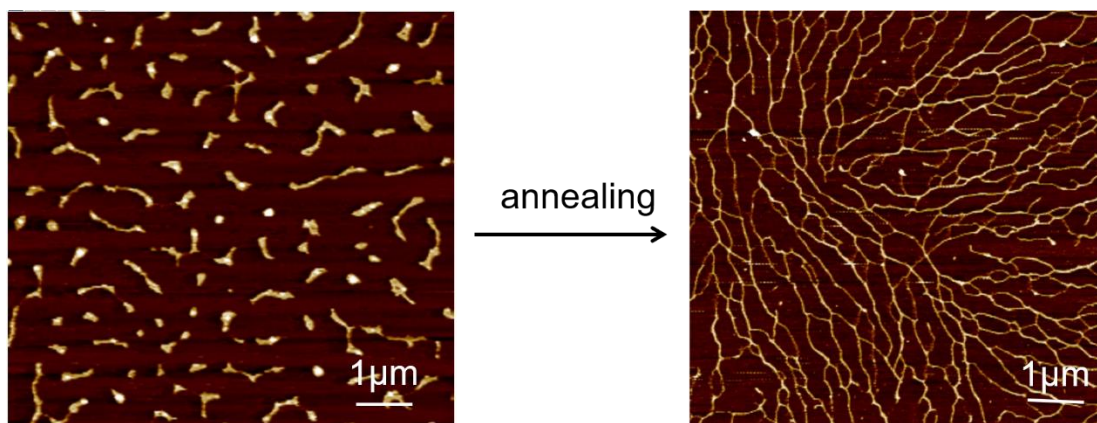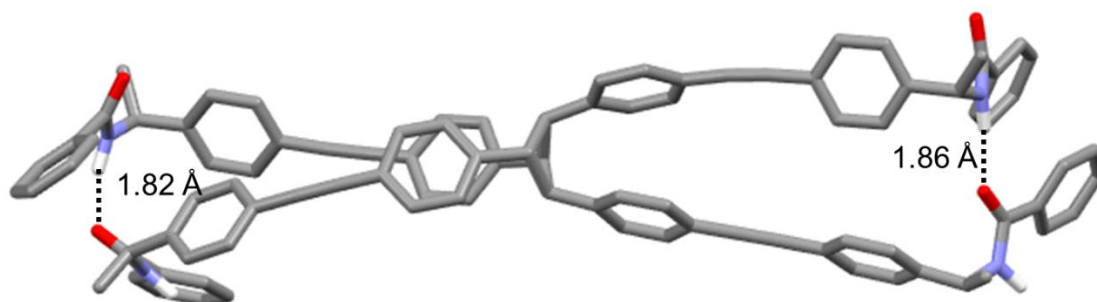

Fig. S19 AFM phase images of (*S*)-**2**k and (*S*)-**2**sp (drop-casted from MCH solution on mica). Scale bar: 1 *μ*m.

Fig. S20 FT–IR spectra of the N–H stretching vibration of (*S*)-**2**$_{monomer}$, (*S*)-**2**$_k$ and (*S*)-**2**$_{sp}$ in MCH at 298 K (*c* = 5.00 mM). The N–H stretching bands shift from 3272 cm^{-1} [(*S*)-**2**$_k$] to 3290 cm^{-1} [(*S*)-**2**$_{sp}$].


Fig. S21 Optimized structures of (*S*)-**2**$_k$ based on DFT calculations. Structural optimization yielded a [2 + 2] cycloaddition species with a folded conformation. This species exhibited two intramolecular hydrogen bonds with N–H···O bond lengths of 1.82 and 1.86 Å.
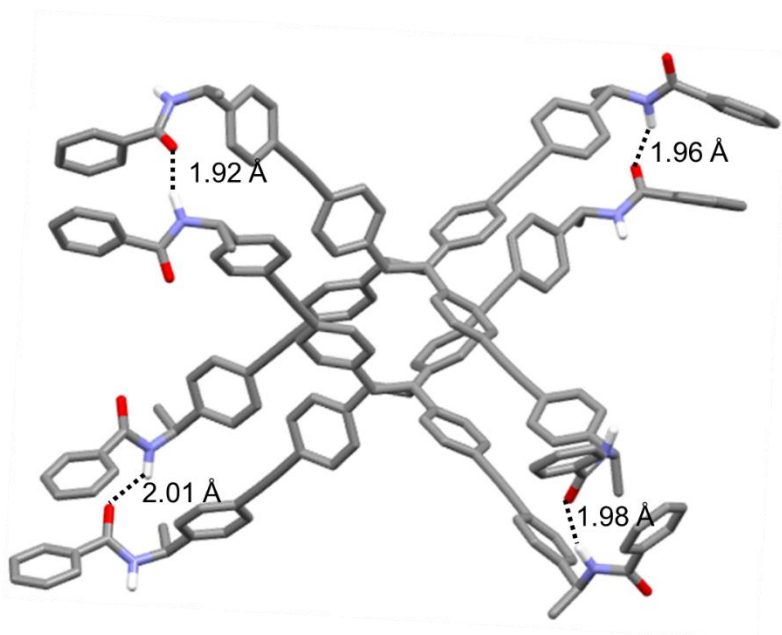
Fig. S22 Optimized dimeric structures of (*S*)-**2**$_{sp}$ based on DFT calculations. The N–H---O bond lengths in (*S*)-**2**$_{sp}$ ranged from 1.92 to 2.01 Å, relatively longer than those in (*S*)-**2**$_k$.
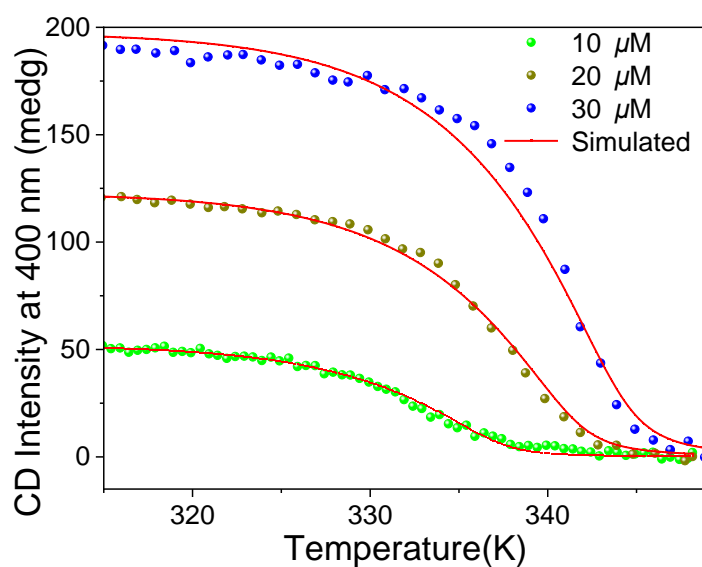
Fig. S23 Experimental (circles) and simulated (lines) CD heating curves of the supramolecular polymerization of (*S*)-**2**$_{sp}$ at three different concentrations (*c* = 10 μM, 20 μM, 30 μM in MCH). The heating rate was 1 K min^{-1}. The $\Delta H_{(S)\text{-}2}$, and $\Delta S_{(S)\text{-}2}$, $\Delta G_{(S)\text{-}2}$ values were determined to be –149.2 kJ mol^{-1}, –348 J mol^{-1} K^{-1}, –45.5 kJ·mol^{-1} respectively.
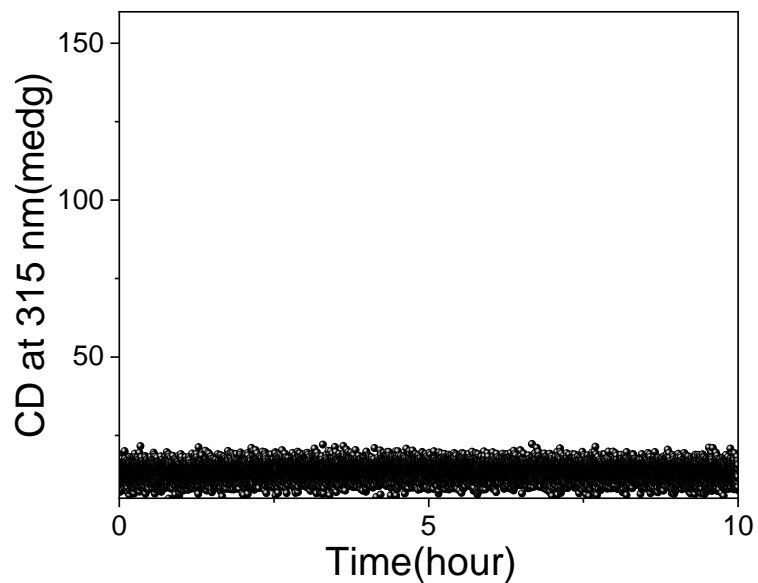
Figure S24 Plot of CD intensity of (*S*)-**2**$_k$ *versus* time at 315 nm in MCH (c = 20 μM, 298 K). No CD changes were observed for at least 12 hours at 298 K, indicating a high activation energy of dissociation.
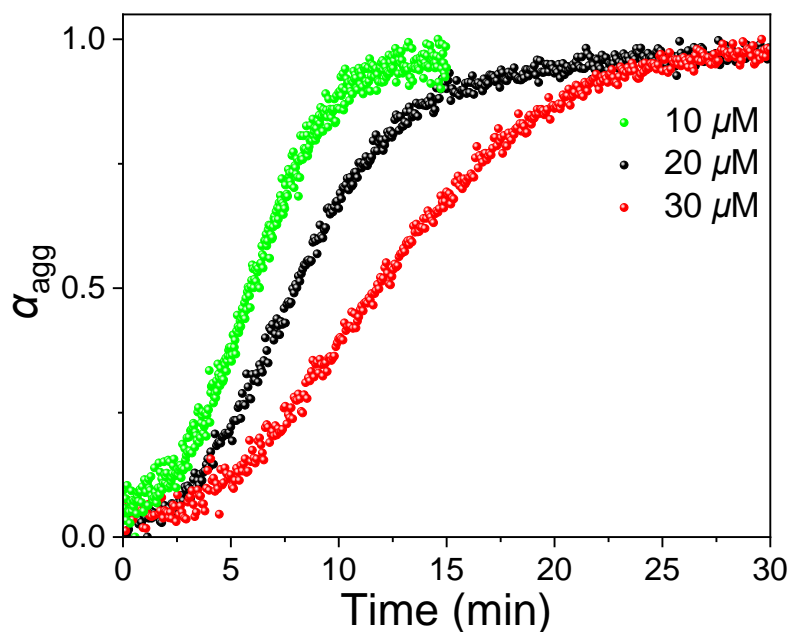
Fig. S25 Plot of CD intensity of (*S*)-**2**$_k$ *versus* time at 315 nm in MCH (323 K) at different concentrations. It represents an "off-pathway" aggregate, which disassembles into the monomeric state before assembling into the thermodynamically stable aggregate (S)-**2**$_{sp}$.

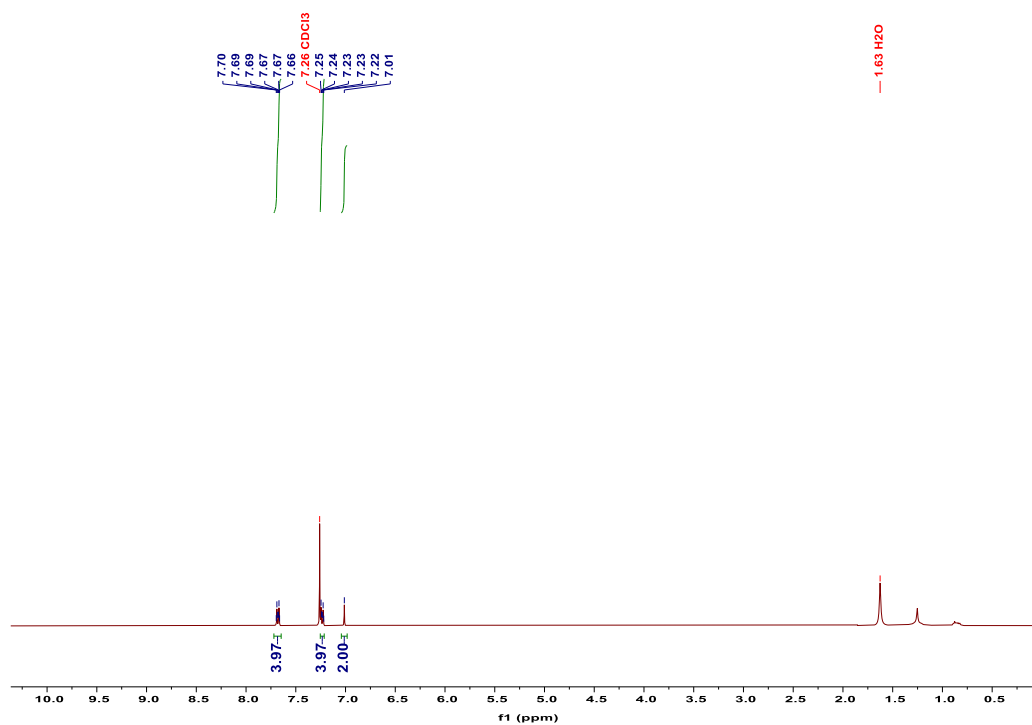# 5. *Structural characterization of the synthetic compounds*

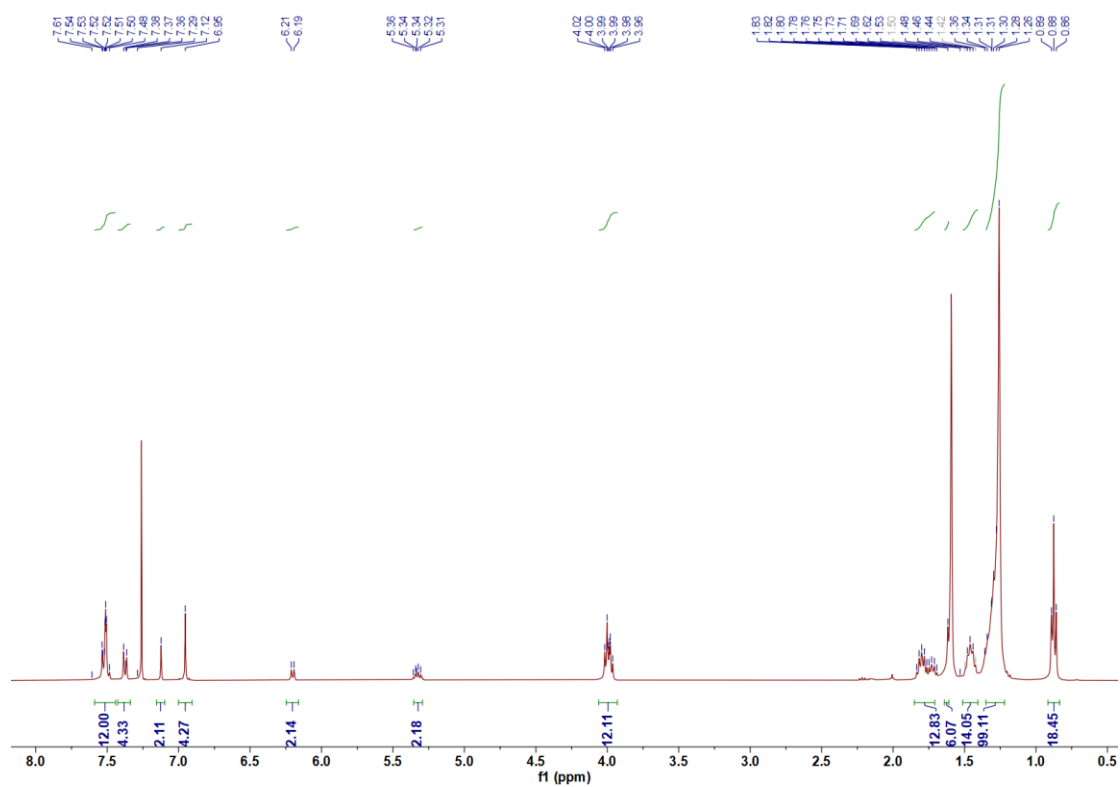**Fig. S26** ^{1}H NMR spectrum (400 MHz, CDCl$_3$) of *trans*-1,2-bis(4-iodophenyl) ethene.

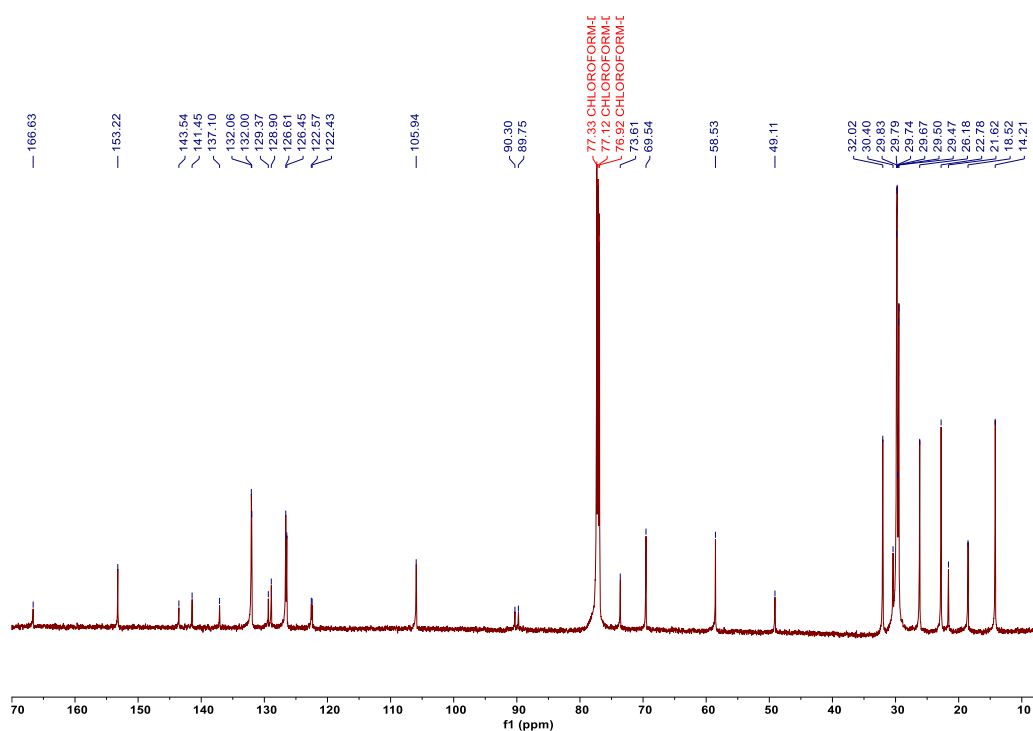**Fig. S27** ^{1}H NMR spectrum (400 MHz, CDCl$_3$) of (*S*)-**1**.

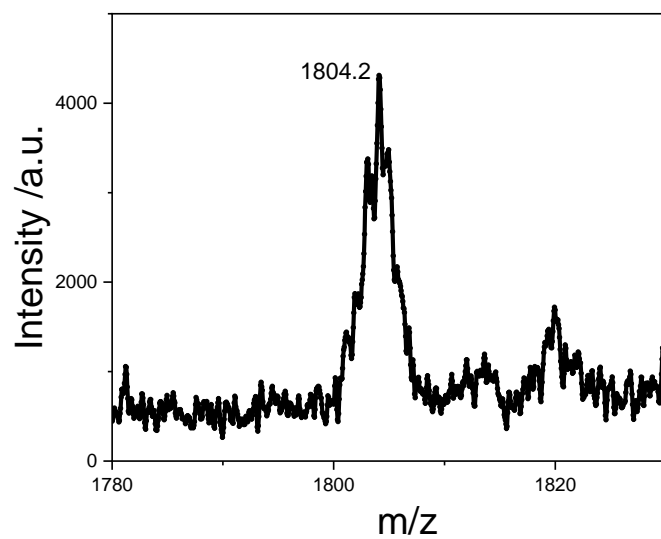**Fig. S28** ^{13}C NMR spectrum (101 MHz, CDCl$_3$) of (*S*)-**1**.
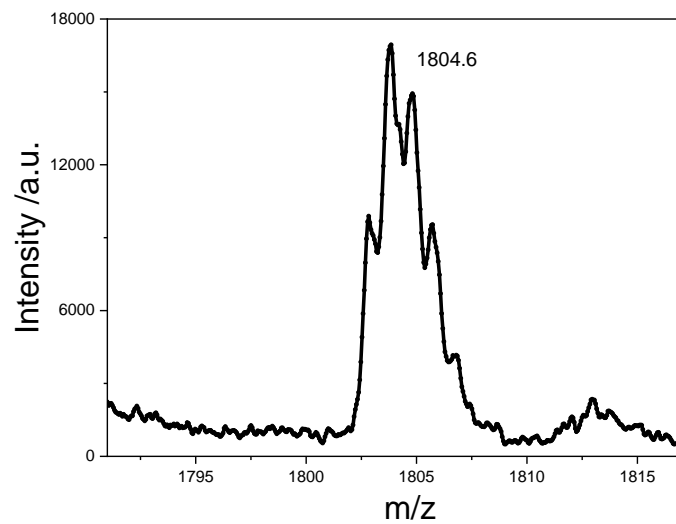

Fig. S29 MALDI-TOF mass spectrum of (*S*)-**1**.
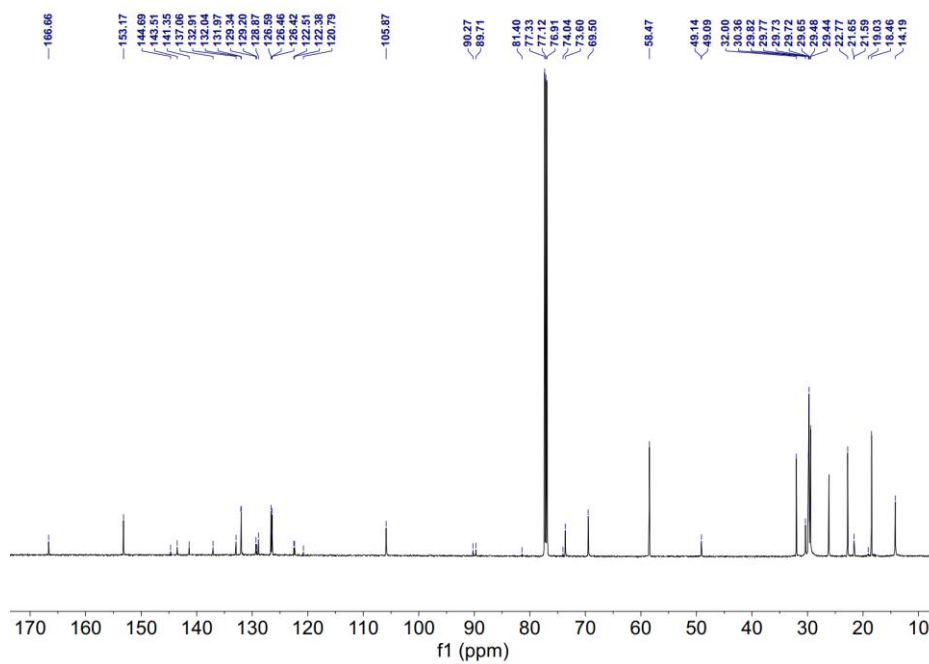
Fig. S30 MALDI-TOF mass spectrum of (*R*)-**1**.

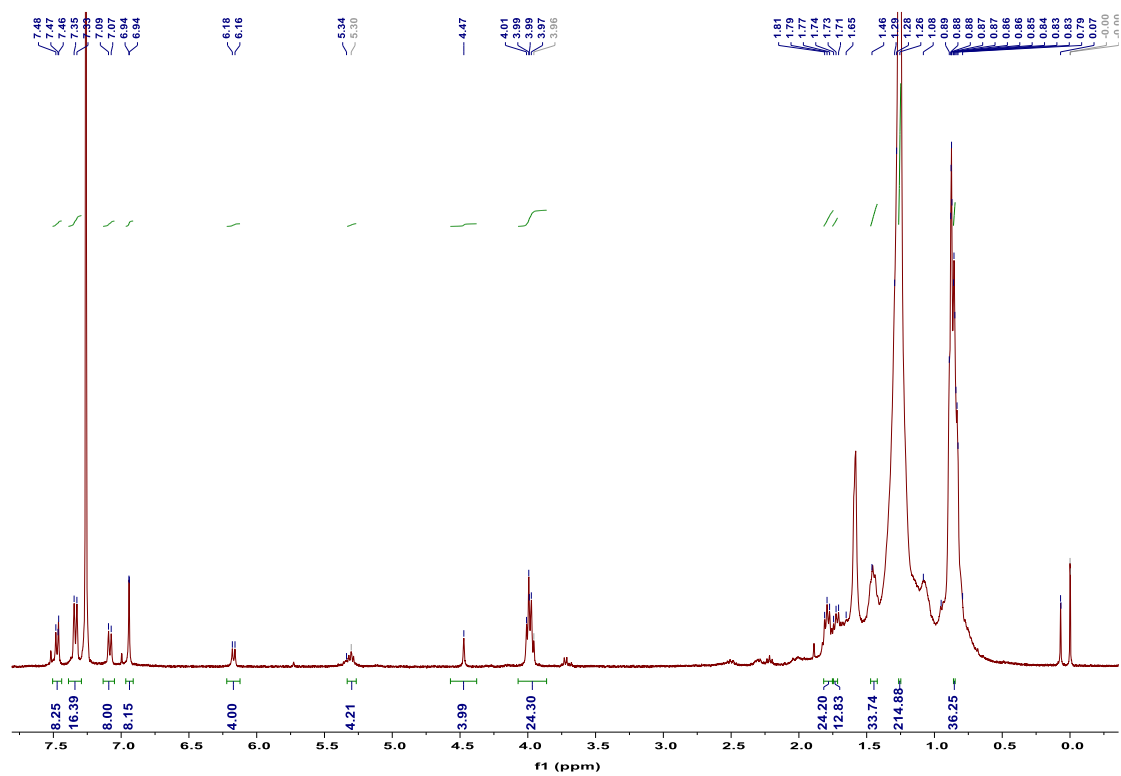**Fig. S31** ^{13}C NMR spectrum (400 MHz, CDCl$_3$) of (*R*)-**1**

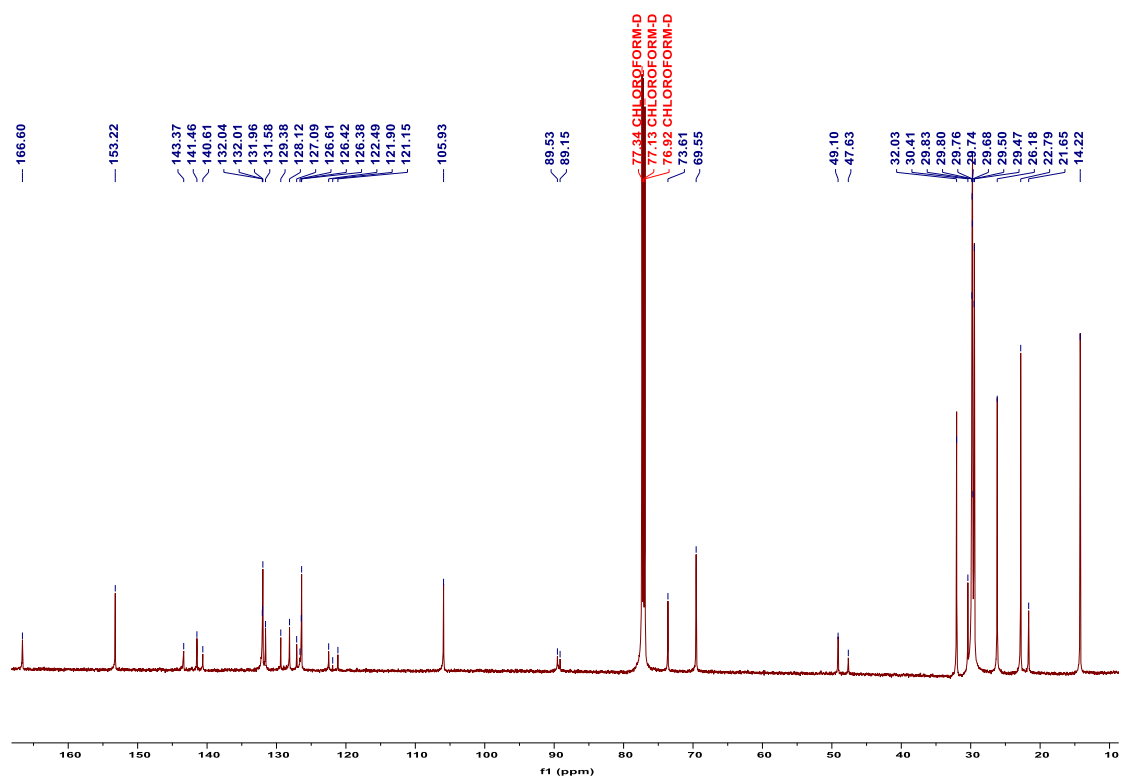**Fig. S32** ^{1}H NMR spectrum (400 MHz, CDCl$_3$) of (*S*)-**2**

Fig. S33 ^{13}C NMR spectrum (101 MHz, CDCl$_3$) of (*S*)-**2**.

References

(S1) X. Li, J. Cui, Q. Ba, Z. Zhang, S. Chen, G. Yin, Y. Wang, B. Li, G. Xiang, K. Kim, H. Xu, Z. Zhang, H. Wang, *Adv. Mater*. **2019**, 31, 1900613.

(S2) R. Liao, F. Wang, Y. Guo, Y. Han, F. Wang, *J. Am. Chem. Soc*. **2022**, 144, 9775–9784.

(S3) Y. Xue, C. Zhang, T. Lv, L. Qiu, F. Wang, *Angew. Chem. Int. Ed.* **2023**, 62, e202300972.

(S4) (a) J. J. P. Stewart, Optimization of parameters for semiempirical methods VI: more modifications to the NDDO approximations and reoptimization of parameters. *J. Mol. Model.* **2013**, 19, 1–32. (b) J. P. S. James, MOPAC2016; Stewart Computational Chemistry. http://openmopac.net/.

(S5) D. Zhao, J. S. Moore, *Org. Biomol. Chem.* **2003**, *1*, 3471-3491.

(S6) M. M. J. Smulders, A. P. H. J. Schenning, E. W. Meijer, *J. Am. Chem. Soc.* **2008**, *130*, 606–611.